Journal of Biological Physics **29:** 201–218, 2003.

Biological and Biomedical Applications of Synchrotron Infrared Microspectroscopy

P. DUMAS[1] and L. MILLER[2]
[1]*LURE – Bat 209D – Centre Universitaire Paris-Sud, F–91898 Orsay cédex, France*
[2]*National Synchrotron Light Source, Building 725D, Brookhaven National Laboratory, Upton, NY 11973-5000, USA*

Abstract. The high brightness of synchrotron light, which is about three orders of magnitude greater than a thermal source, has been exploited in biological and biomedical applications of infrared microspectroscopy. The potential of this analytical tool is documented in this article in the study of human tissue (hair and skin) and individual cells: biochemical and bio-structural changes based on corresponding functional groups have been identified and imaged with unprecedented spatial resolution. This technique also provides a new tool for analysis of biochemical kinetics of samples during disease and treatment. In the future, the combination of infrared microspectroscopy with other synchrotron-based microscopic techniques, such as X-ray microscopy, at the same sample location is discussed.

Key words: cells, hair, infrared, microscopy, microspectroscopy, skin, synchrotron, x-ray

1. Introduction

Infrared absorption bands observed in the mid-IR (MIR) region, between approximatively 400 and 4000 cm^{-1} (11.9 to 119 THz), arise mainly from vibrational modes of particular molecular motions. At wavenumbers lower than typically 1400 cm^{-1} ($\sim$42 THz), IR absorption modes tend no longer to arise from localized vibrational motion, but rather from skeletal and strongly coupled modes.

FT-IR microspectroscopy, i.e. the combination of FT-IR spectroscopy and microscopy, has proven to be an attractive analytical technique, and applications in the biological and biomedical fields (intact microbial plant or mammalian cells, tissues and body fluids) have grown rapidly [1]. The primary reason is that many common biomolecules, such as nucleic acids, proteins, lipids, and carbohydrates have characteristic and well-known vibrational fingerprints. In fact, many biological samples have highly specific vibrational signatures that form a database for discriminating various states [2–8].

Since biological samples are heterogeneous and complex, the diagnostic potential of biochemical identification strongly depends on the quality of the spectra acquired, i.e. signal-to- noise and lateral resolution. Present day FTIR spectrometers and microscopes are well matched and deliver high performance. Spatially resolved

infrared spectroscopy allows the production of images of the chemical composition and distribution within complex and heterogeneous biological samples. Functional groups mapping is the most common method for chemical imaging of samples, but more sophisticated pattern recognition techniques, such as factor analysis, hierarchical clustering, and Artificial Neural Network (ANN), are becoming more popular [4, 9].

Still, signal-to-noise requirements often limit the smallest practical spot size to $\sim$20 μm. This limitation is not the consequence of diffraction or aberration in the optical system of the IR microscope, but rather due to the low intrinsic brightness (defined as the photon flux or power emitted per source area and solid angle) of the thermal infrared source. Higher brightness infrared sources do exist (e.g. lasers), but the synchrotron source is the only broadband source that delivers the entire infrared wavelength range (from far-IR to near-IR) [10]. It is worth noting that the brightness advantage of this source is not because the synchrotron produces more power, but because of the small source size and narrow ranges of angles of emission.

The use of a synchrotron source in infrared microspectroscopy has benefited to biologists significantly, but applications are still in their infancy. This paper illustrates the potential offered by synchrotron-powered infrared microspectroscopy in biology. In addition, since the IR microscope is operated at a synchrotron facility, other synchrotron-based microanalytical tools, particularly X-ray microscopy can be used to probe the same sample area.

2. Infrared Synchrotron Radiation and Advantages in Microspectroscopy

Electrons in linear accelerators and storage rings are accelerated in bunches by radio-frequency cavities. The light that is emitted is given by the incoherent superposition of the emission from a single electron, where the intensity of the emitted light is proportional to the number of electrons in the bunch [11]. Radiation is emitted either by the longitudinal, or the transverse, velocity change of the electrons entering or exiting dipoles. Longitudinal radiation (edge radiation) is emitted into angles close to $\frac{1}{\gamma}$ (where γ ratio of the mass of the electron to the rest mass), much smaller than in the case of transverse radiation. However, the emitted power and the brightness of the radiation are the same order of magnitude, which is illustrated in Figure 1. This figure shows the intensity distribution (Figures 1a and 1b) at a wavelength of 10 μm (1000 cm^{-1}) for a storage ring with an energy of 2.75 GeV, a stored current of 400 mA, and an extraction geometry of 20 mrad (vertical) $\times$ 30 mrad (horizontal). It can be seen from Figures 1a and 1b that the infrared photons from the edge radiation are emitted into a narrower angular distribution compared to those from the bending magnet. Figure 1c shows the calculated power (in watts per 0.1% bandwidth), for the two types of sources. They are quite close, but as can be seen in Figures 1a and 1b, the total power extracted can be improved in the case of bending magnet radiation, by enlarging both the vertical and horizontal apertures

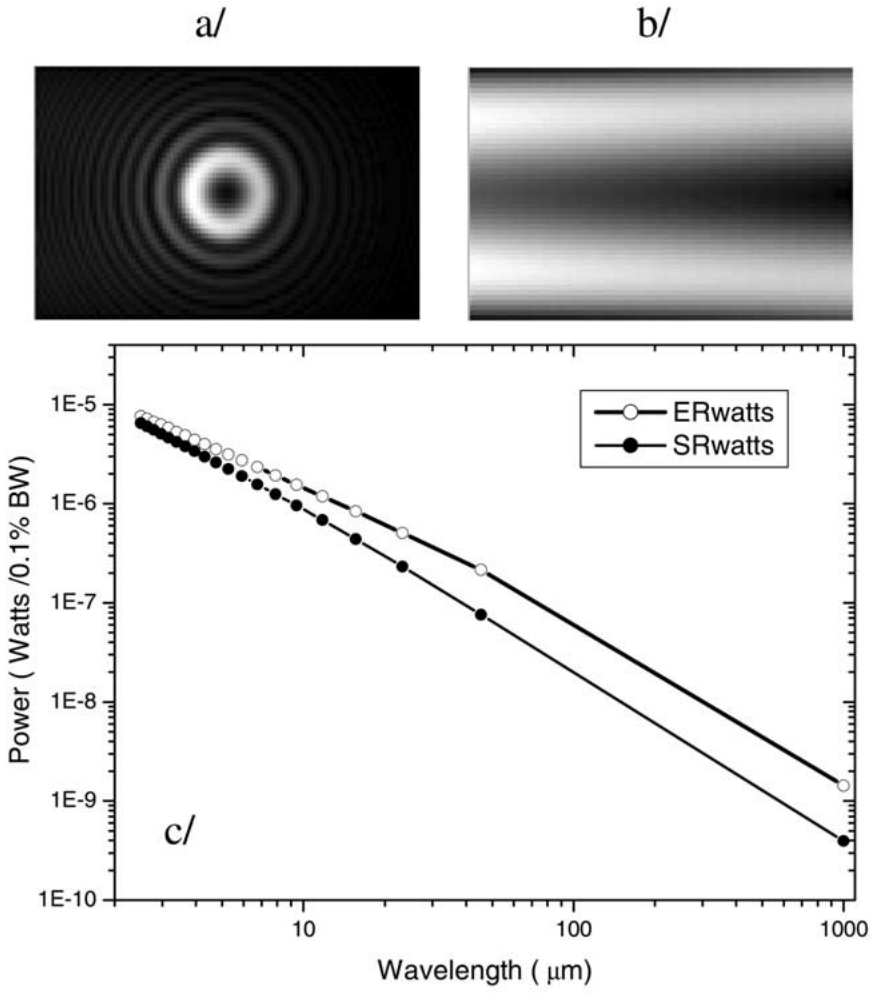

Figure 1. Calculated infrared emission from a synchrotron source, using the SRW code [12] and for the following parameters: electron energy = 2.75 GeV, electron current = 400 mA, magnetic field = 1.56T, straight section length = 7 meters, distance to point source = 2.3 meters, collection angles: 30 mrad (Horizontal) × 20 mrad (Vertical). **(a)** Intensity profile for an edge radiation; **(b)** intensity profile for the bending magnet collected at 4° deviation; **(c)** power emitted by the two sources at a function of wavelength (expressed in Watts per 0.1% bandwidth (BW)). Open circles are for edge radiation, black dots are for bending magnet radiation.

(which often requires modification of the dipole vessel of existing facilities). Calculations reported in Figure 1 have been performed using the SRW computer code from Chubar and Elleaume [12]. However, for the case of the bending magnet, a simplified formula can be used to calculate the emitted power and brightness (also called brilliance, or spectral radiance) [13, 14].

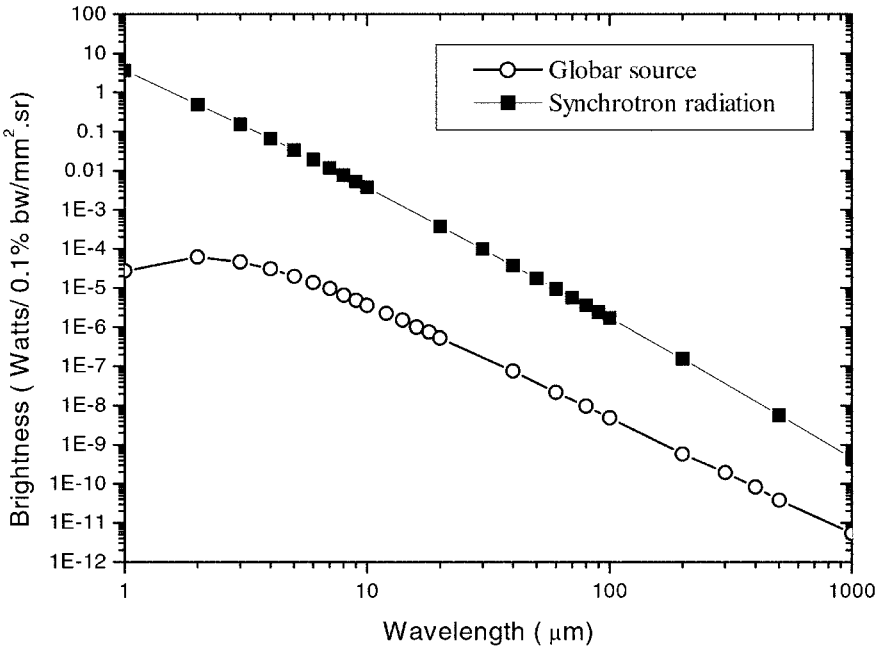

Figure 2. Calculated brightness for a blackbody at 2000 K and bending magnet infrared emission (electron energy= 2.75 GeV, electron current= 400 mA, bending magnet radius= 5.36 meters).

The power emitted by a thermal source, traditionally found in any commercial spectrometer, has the following equation:

$$P_{bb}(Watts) = \frac{2\pi hc^2}{\lambda^5} \frac{d\lambda}{e^{\frac{ch}{\lambda KT}} - 1} \tag{1}$$

where is the power emitted per unit surface area, λ is the wavelength in microns, h, k, and c are Planck's constant, Boltzman's constant, and the speed of light, respectively. ($2\pi hc^2 = 3.7415\times 10^{-16}$ W/m^2; $hc/k = 1.4387\times 10^{-1}$ m.K). The brightness of a thermal source can be easily calculated by dividing by $2\pi \times$ (emitted area).

According to Williams [13, 14], the synchrotron radiation power is approximated as (for a bending magnet):

$$P_{SRS}(\lambda) = 4.38 \times 10^{14}.I.\theta.bw(\rho/\lambda)^{1/3} \tag{2}$$

where I is the stored current (in Amperes), θ the horizontal collection angle, bw is the bandwidth (in %), λ the wavelength in microns, and ρ the radius of the storage ring (in meters). $P(\lambda)$ is expressed in photons per second, but can be converted to Watts by dividing by $5.04 \times 10^{18}.\lambda$. Accordingly, the approximate infrared brightness of a storage ring is given by:

$$B(\lambda) = 75.I.bw/\lambda^3 \text{ in W/mm}^2\text{/sr} \tag{3}$$

Figure 2 compares the calculated brightness for the same parameters of the storage ring (cf. Figure 1). As can be seen, a brightness advantage of roughly three orders of magnitude is achieved with the synchrotron source.

This advantage is well illustrated for microspectroscopy. The IR spectrum of an individual human cell is shown in Figure 3 using a 6×6 μm^2 aperture (1000 accumulations) with a blackbody source, and with a 3×3 μm^2 aperture using the synchrotron source (32 accumulations). The signal-to-noise of the synchrotron data is clearly superior to that of the thermal source. In addition, despite of the much higher brightness, there is negligible heating of sample, which is important for biological tissue [15].

3. Synchrotron IR Microscopy and Applications in Biology and Biomedicine

3.1. INSTRUMENTATION

Infrared microscopy is the combination of an optical microscope with a FTIR spectrometer bench. The spatial resolution is achieved by constraining the illuminated region, thanks to an adjustable aperture placed at an intermediate focal point, and re-imaged the aperture size onto the sample, using generally Schwarzschild objectives, of various magnifications.

In the current studies, a Nic-Plan IR microscope (coupled to a Magna 560 FTIR spectrometer) and a Continuum IR microscope (coupled to a Nicolet Magna 860 FTIR spectrometer) were used. They were operated in confocal mode, where the focusing Schwarzschild objective had a magnification of 32x (NA=0.85) and the collection Schwarzschild objective had a magnification of 10x (N.A. = 0.71). The area of illumination was determined with an adjustable aperture placed at an intermediate focal point, and re-imaged onto the sample. The upper and lower apertures are adjustable to approximately 3×3 μm^2. The microscopes were connected to synchrotron beamlines at LURE (France; Beamline MIRAGE) [16] and the National synchrotron Light Source (BNL, USA; Beamline U10B) [17].

In the following applications, spectra were collected in transmission mode, at either 8 cm^{-1} or 4 cm^{-1} resolution using Atlμs software (Thermo Nicolet Instruments). Area mapping was performed using a dual remote masking aperture to define the sample area for infrared data collection and minimize diffraction. The final format of the data was absorbance, where the background was collected through the blank substrate.

3.2. INFRARED SPECTRA OF BIOLOGICAL SAMPLES

Efforts to interpret the IR spectra of biological molecules are mainly based on the analysis of known structures, normal coordinate analysis and isotope exchange experiments [18]. Nucleic acids, proteins, lipids and carbohydrates are constantly present in different proportions and wide diversity. Examples of their IR spectra are displayed in Figure 4. The proportion of the relative components may vary.

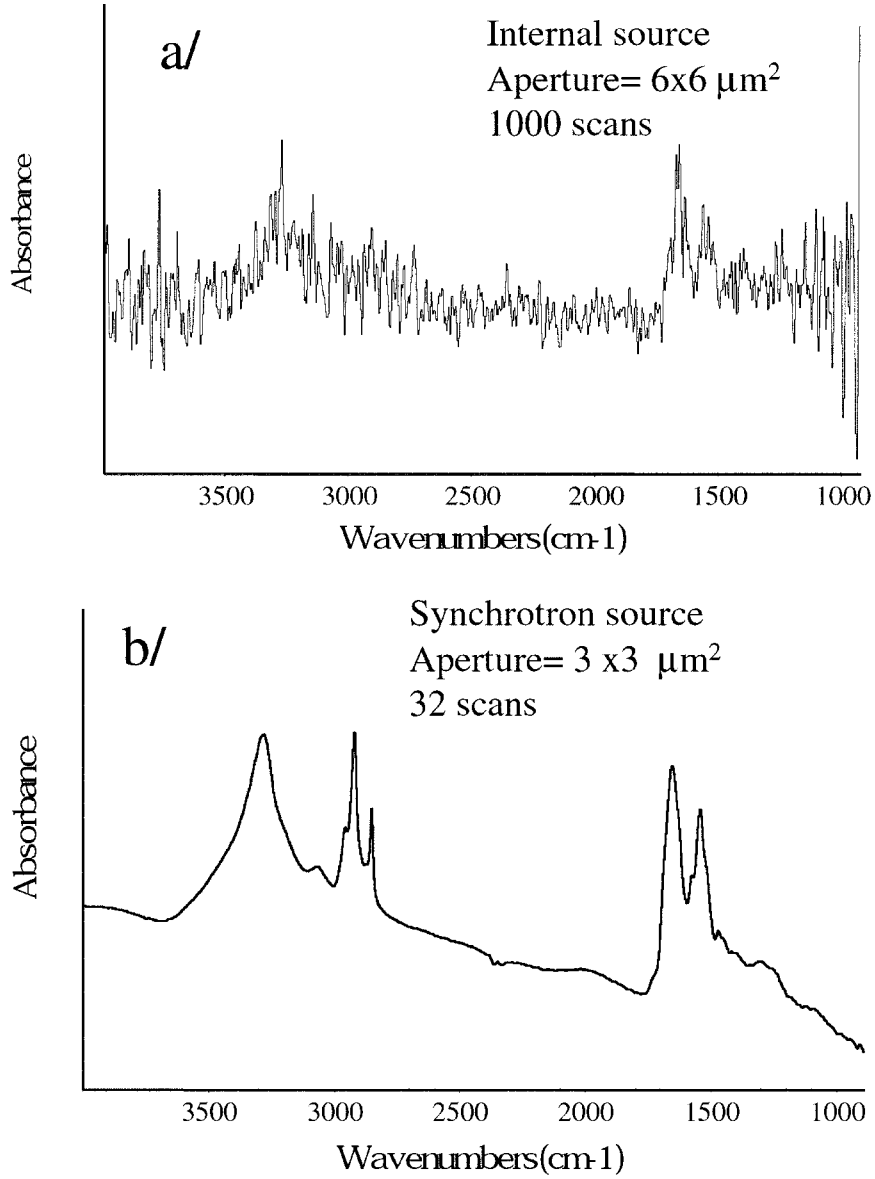

Figure 3. The IR spectra of an individual human cell **(a)** using a 6×6 μm^2 aperture (1000 accumulations) with a blackbody source, and **(b)** using a 3×3 μm^2 aperture with the synchrotron source (32 accumulations).

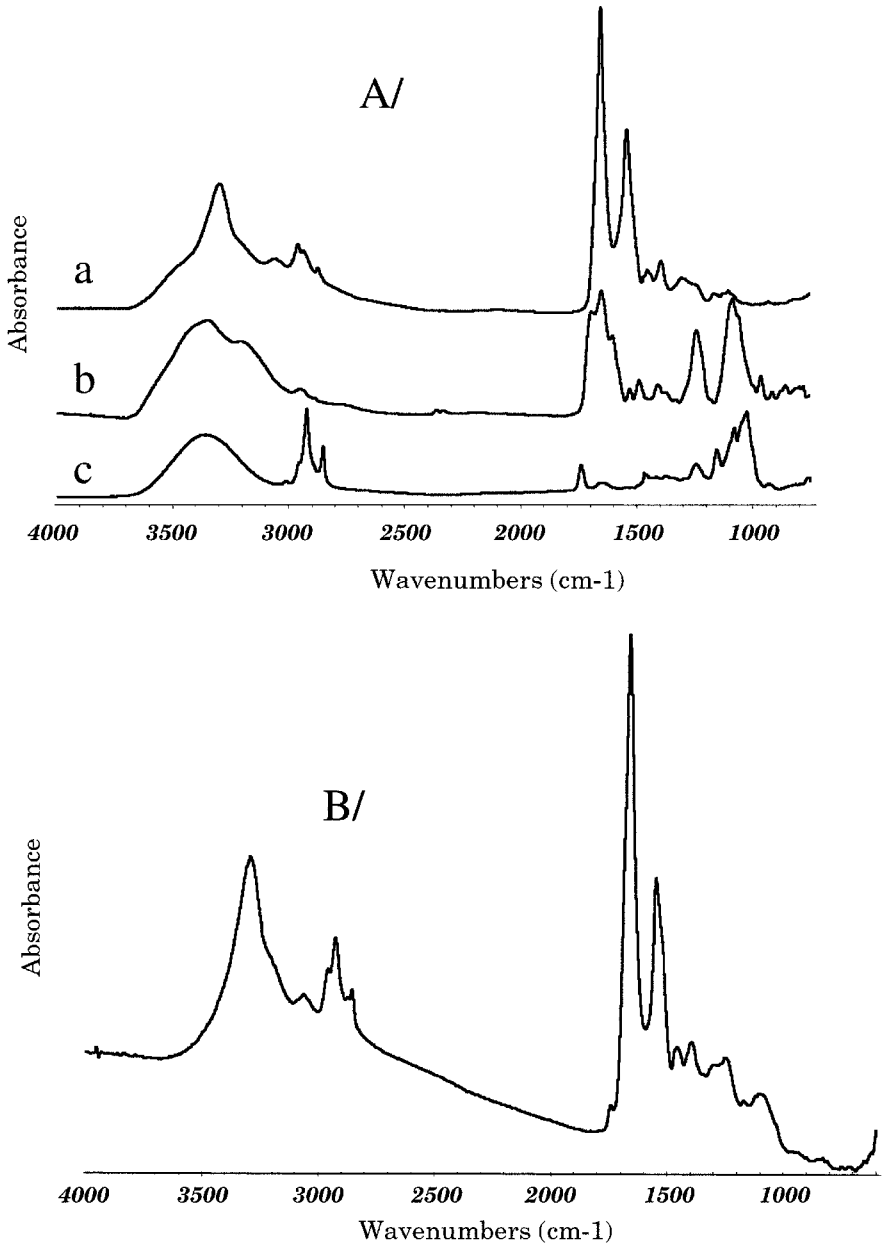

Figure 4. Typical infrared spectra of biological tissues and main components. **(A)** IR spectra of (from top to bottom) a protein (a), nucleic acid (b), and phospholipid (c). **(B)** Typical spectrum of a biological sample. Depending upon the relative component concentrations in the tissue, the spectrum can vary in relative intensity between the bands.

Table I. Tentative assignment of bands frequently found in biological samples [4]

Frequency ($\sim cm^{-1}$)	Assignment
~3500	O-H stretch of hydroxyl groups
~3200	N-H stretch (Amide A) of proteins
2959	Asymmetric C-H stretch of – CH_3
2934	Asymmetric C-H stretch of – CH_2
2921	Asymmetric C-H stretch of – CH_2 of fatty acids
2898	C-H stretch of C-H methine
2872	Symmetric C-H stretch of – CH_3
2852	Symmetric C-H stretch of – CH_2 of fatty acids
1741	$\rangle$ C=O str. of esters
1715	C=O str. of esters, RNA/DNA, $-C\leq^{O}_{O\text{-}H}$
1695, 1685, 1675	Amide I band components resulting from antiparallel pleated sheets and β-turns of proteins
~1655	Amide I of α-helical structures
~1637	Amide I of β-pleated sheet structures
1575	Asymmetric stretch ν_{AS} COO^-
1548	Amide II
1515	'tyrosine' band
1468	C-H deformation of CH_2
~1400	Symmetric C=O str. of COO^-
1310–1240	Amide III band components of proteins
1250–1220	Asymmetric P=O str. of PO_2^- phosphodiesters
1200–900	C-O-C, C-O dominated by ring vibrations of carbohydrates C-O-P, P-O-P
1085	Symmetric P=O str. of PO_2^- phosphodiesters
720	C-H rocking of CH_2
900–600	'Fingerprint region'

Figure 4b shows a typical spectrum of a biological sample. Table I reports the main vibrational features observed and their assignments, according to the literature [4].

IR microscopy at higher spatial resolution is mainly intended to detect slight difference in band intensity or position (uni-variate change) or overall spectral changes (multivariate analysis). An important feature of biological IR spectra is the lineshape of the so-called Amide I region, extending between 1580–1700 cm^{-1}. The secondary structure of proteins can be inferred by the careful analysis of the various components of this massif [3] (see also Table I).

3.3. SYNCHROTRON INFRARED MICROSCOPY OF HUMAN HAIR

Human hair is 50–100 μm in diameter and its cross-section reveals three major identifiable regions. The medulla is the center-most portion of the hair. It is 5–10 μm in diameter and composed of loosely packed, keratinized cells that distribute moisture and nutrients to the hair strand. The medulla can be either continuous or discontinuous along the hair length, and often it is completely absent. The cortex makes up the bulk of a hair fiber and determines the strength of a hair. It is 45–90 μm in diameter and composed of long embedded cortical cells; it also contains the hair pigment, melanin. The outermost layer of a hair strand is the cuticle, which is less than 5 μm in thickness. It is a dense layer of flat keratinized cells, which protects the hair fiber. As far as composition is concerned, vibrational microspectroscopy seems to be a perfect tool in hair research.

In this study, hair samples were collected from virgin hair obtained from young Caucasian females. Hair samples were embedded in Tissue-Tek (Reichert-Jung, Heidelberg-Germany) product. Cross-sections were cut at a thickness of 5 μm using a cryomicrotome (MICROM). The blades were cleaned between each pass to prevent contamination on the section. Infrared spectra were collected either with a 6×6 μm^2or a 3×3 μm^2 aperture. For the data reported here, IR spectra were recorded with a resolution of 4 cm^{-1}, and either 32 or 64 scans were co-added before Fourier transform processing. A linear baseline subtraction was performed on each spectrum, to account for the gradual decay of the beam intensity in the synchrotron source. Then, the heights of selected peaks or integrated areas were calculated for each spectrum.

IR spectra of the medulla, cortex and cuticle, are shown in Figure 5. There are significant differences in the spectral signatures in each region. Inside the medulla, a higher intensity of CH_2 stretch is observed, together with additional bands at 1740 cm^{-1}, 1575 cm^{-1} and 1469 cm^{-1} (see enlarged frequency region in Figure 5b). The band at 1740 cm^{-1} is assigned to a C=O ester group, while the bands at 1576 and 1469 cm^{-1} are attributed to the ν_{AS} and ν_{SS} modes of COO^- (i.e. carboxylic acid salts) (see Table I). In addition, the Amide I frequency region (between 1585 and 1710 cm^{-1}) is significantly different between the three hair regions, in both line shape and the Amide I peak position. This suggests differences in secondary structure composition of the proteins in each region [3].

The chemical distribution of lipids in the hair cross-section, was shown to be highly localized inside the medulla [19]). By using an aperture size of 3×3 μm^2, and steps of 2 μm, we have obtained a much detailed chemical profile inside the medulla (Figure 6). Clearly, the methylene (Figure 6a), the COO- (Figure 6c) and the ester C=O groups (Figure 6d) are concentrated in the medulla, concomitant to a lower proteins content (Figure 6b).

The distribution of protein secondary structure within the hair cross-section was also imaged. By ratioing the absorbance at 1630 cm^{-1} (characteristic of pleated β-

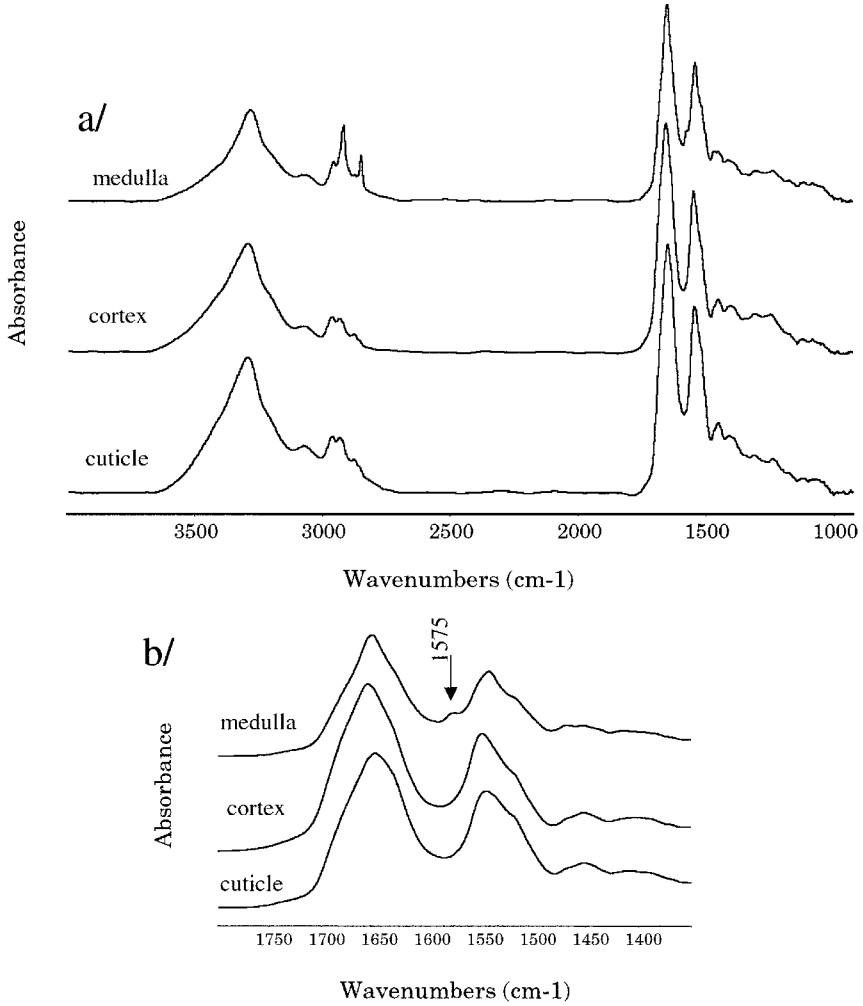

Figure 5. **(a)** Infrared spectra of the medulla, cortex, and cuticle of a Caucasian hair section (6 μm in thickness), 64 scans recorded with an aperture of 6×6 μm^2 **(b)** Enlargement of the Amide I and II region from (a), showing the presence of an additional band at 1575 cm^{-1} inside the medulla, and the different line shape of the Amide I band.

sheets) to that at 1655 cm^{-1} (characteristic of α-helical structure), a higher ratio of β-sheet structure is evident in the cuticle (Figure 7).

This analysis demonstrates the analytical potential of synchrotron-powered IR microspectroscopy to study hair composition. Apart from a detailed characterization of the biochemical composition and secondary structure, the study of the effects and penetration pathway of external agent has also been initiated [20, 21].

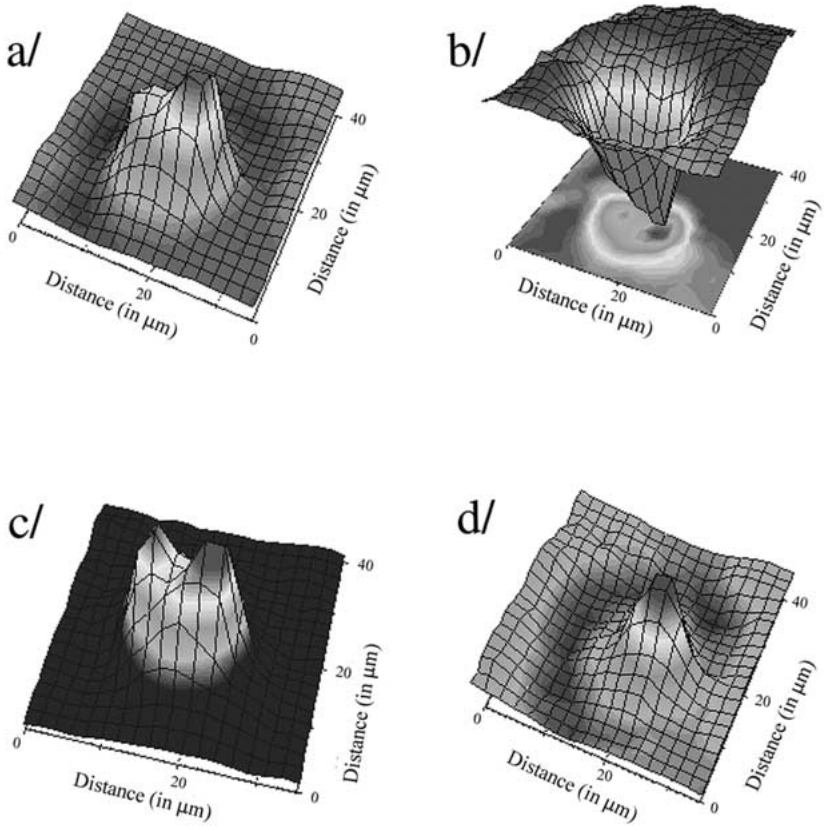

Figure 6. Chemical distribution of **(a)** lipid characteristics vibrational band (CH_2 asymmetric stretch at 2929 cm^{-1}); **(b)** protein characteristic band (Amide I band); **(c)** COO^- frequency at 1576 cm^{-1} and **(d)** C=O ester frequency at 1736 cm^{-1}. These images result from the analysis of IR maps taken in 2 μm steps, with an aperture of 3×3 μm^2, 4 cm^{-1} resolution, 64 scans.

3.4. SYNCHROTRON INFRARED MICROSCOPY OF HUMAN SKIN

Infrared microspectroscopy has demonstrated its advantages in the analysis of skin composition and investigating its disorders, especially for the detection of basal cell carcinoma [22, 23]. The detailed analysis of the biomolecular composition and protein secondary structure of the Stratum Corneum (SC) have important implications for understanding the barrier function of the skin's outmost layer. On average, human SC is 10 to 20 μm in thickness, and consists of flattened, anucleated and protein-rich cells embedded in a multilamellar lipid matrix mainly composed of ceramides [24]. It is believed that the penetration pathway is controlled by the intercellular lipid domain [24]. For pharmaceutical purposes, understanding the

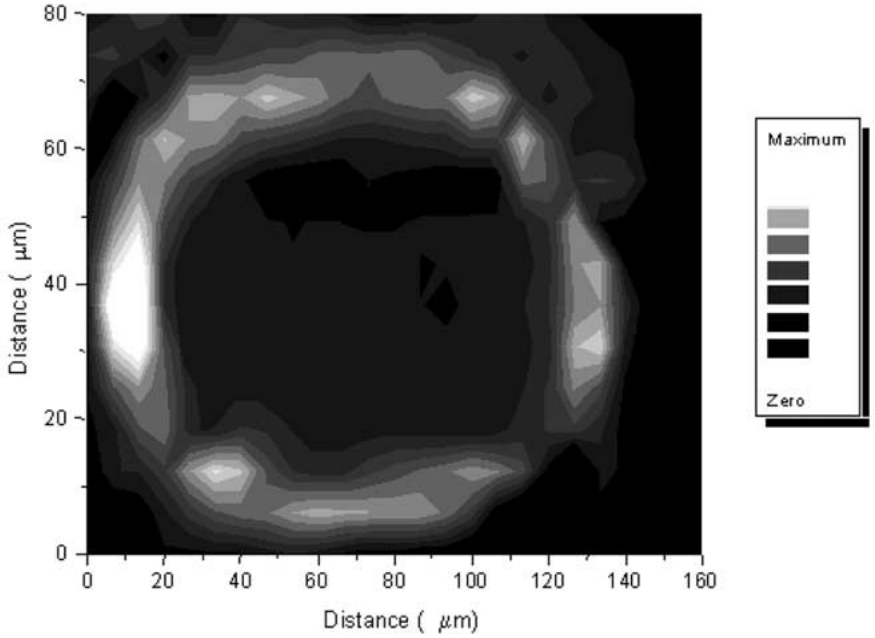

Figure 7. Intensity profile of the Amide I ratio: 1630 cm^{-1}/1655 cm^{-1}, recorded with an aperture of 6×6 μm^2, 32 scans and 4 cm^{-1} resolution. The highest values are located inside the cuticle.

biochemical and biophysical properties of SC lipids is of paramount importance for developing strategies to enhance the transdermal penetration.

In this work, synchrotron infrared studies of skin have been performed on human explants. Thin sections (7 μm) were obtained from frozen tissue blocks embedded in Tissue-Tek. They were placed onto ZnS windows. Representative spectra, recorded with an aperture of 6×6 μm^2, of the SC, epidermis, and dermis are presented in Figure 8. The CH_2 and CH_3 absorption bands in the SC, between 2800 and 3000 cm^{-1}, differ from those of the dermis and epidermis, both in absolute intensity of the CH_2 stretch modes, and in the CH_2/CH_3 relative intensities. Concomitantly, the band at 1740 cm^{-1} is the highest in intensity in the SC. These results are consistent with the known composition of human skin, i.e. the SC has the highest lipid concentration.

An intensity profile of the lipids, displayed in Figure 9a, shows this high localization. The Amide I intensity, used to monitor the protein distribution, is plotted in Figure 9b. With the highest lateral resolution provided by the synchrotron source, one can more precisely visualize the relative heterogeneous distribution of protein and lipid in human skin sections.

We have identified the highly localization of the phospholipids inside the SC. The effect of the external cosmetic agents on protein secondary structure has been address and will be presented elsewhere [25].

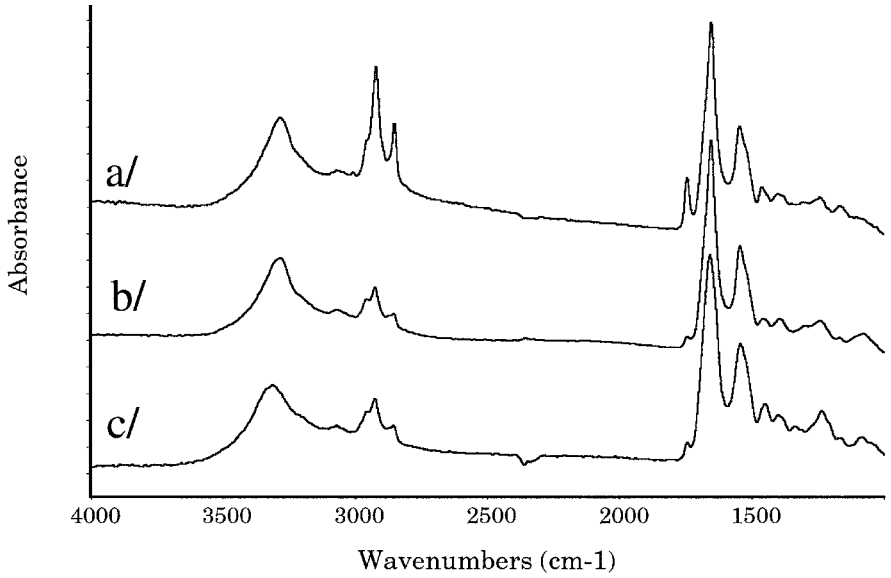

Figure 8. Infrared spectra of different region of human skin, recorded with an aperture of 6×6 μm^2, 8 cm^{-1} resolution and 128 accumulations: **(a)** the stratum Corneum, **(b)** the epidermis, and **(c)** the dermis.

3.5. SYNCHROTRON INFRARED MICROSCOPY OF INDIVIDUAL HUMAN CELLS

Recent papers [26, 27] have shown, for the first time, that synchrotron-based IR microspectroscopy can be used to obtain detailed chemical images of proteins, lipids and nucleic acids in living individual cells, without the use of stains or fixatives. While the identification and mapping of functional groups of an individual living cell appears very challenging, it may offer considerable new insight into the cell's biochemical kinetics during processes such as apoptosis or necrosis.

A recent study of apoptotic cells [28, 29], has shown the marked difference in biochemical composition during the early and late apoptosis. In each state, chemical images have been obtained, showing the role played by each component during the various states. It has also been shown [26, 27], that necrotic (dying) cells exhibit an intense vibrational band at 1740 cm^{-1}, which has been attributed to protein oxidation. With the use of a synchrotron source, the oxidation can be imaged throughout a single cell. This is illustrated in Figure 10, where the protein oxidation is concentrated in the cytoplasm (Figure 10b), while the nucleus (as illustrated by integration of the Amide I band), is unaffected (Figure 10c). The study of cell subcomponents is likely an exciting area for future investigation utilizing the synchrotron source.

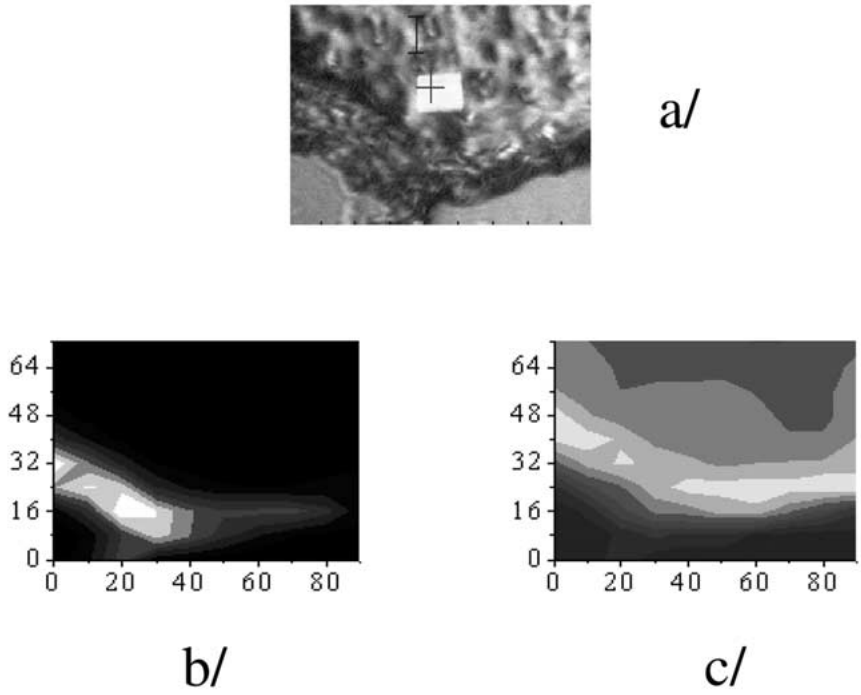

Figure 9. Intensity profile, obtained with a 6×6 μm^2 aperture, of a skin section: **(a)** optical image, **(b)** phospholipid profile at 2920 cm^{-1}, and **(c)** proteins profile (1585 cm^{-1}–1720 cm^{-1}). The phospholipids are highly localized inside the SC.

3.6. COMPLEMENTARITY WITH OTHER SYNCHROTRON-BASED MICROSCOPIC TECHNIQUES

A unique strength of synchrotron-based imaging and microspectroscopy capabilities is the broad range of wavelengths available. With the combined use of bending magnets and insertion devices, the spectrum of produced light extends from the hard x-rays (with wavelengths as small as 0.1 Å), to the far-infrared (with wavelength longer than 10^7 Å). Therefore, a wide array of analytical techniques are available within the same facility: FTIR microspectroscopy, Scanning Transmission X-ray microscopy (STXM), Hard x-ray microscopy, hard-x-ray microprobe analysis, computed x-ray microtomography, Diffraction Enhanced Imaging (DEI), and microbeam x-ray diffraction [30].

Because of the complementarity of these techniques, efforts are underway to combine X-ray microprobe analysis and infrared micro-analysis on the same sample. To illustrate this, identical cross-sections of a hair shaft have been studied with both IR microspectroscopy and X-ray fluorescence microscopy. The hair sections (5 μm thick) were deposited on BaF_2 windows, and analyzed as such at the ID19 beamline, at the European Synchrotron Radiation Facility (Grenoble).

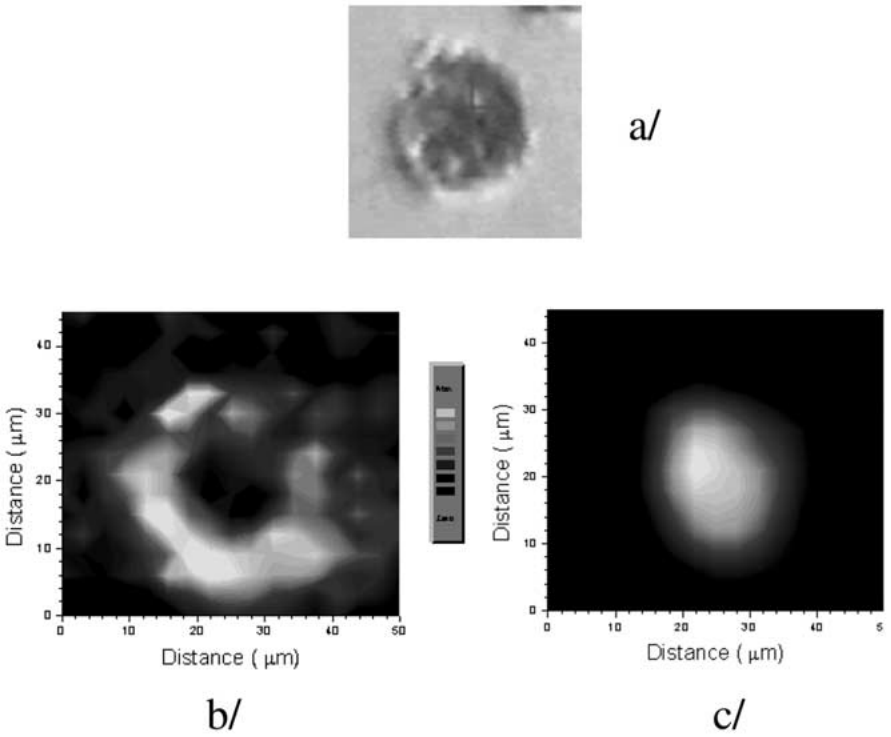

Figure 10. Optical and chemical image of a necrotic single cell. **(a)** optical image,**(b)** chemical image of the C=O band at 1740 cm^{-1}, **(c)** chemical image of the nucleus (Amide I band). The spectra have been recorded with a 3×3 μm^2 aperture, 128 scans and 8 cm^{-1} resolution.

Figure 11a displays the IR intensity profile of the CH_2 stretch mode (i.e. lipids), while Figures 11b, c, and d show the concentration profiles of Ca, S and Cu, respectively. By comparing the images, it can be seen that the medulla contains both a high concentration of lipids and also a high calcium density. We can then infer that calcium based-fatty acidic salts are localized inside the medulla.

The cortex is nicely imaged by the S lesser concentration, and exhibits a lesser concentration inside the medulla, in agreement with the known biochemical composition of hair [31]. Copper is localized inside the cuticle. This will be discussed in a forthcoming paper [32]. Therefore, this example of a combined IR and X-ray microscopy study of a hair section demonstrates the potential of such a combination for future biological or biomedical studies.

4. Conclusion

The brightness advantage of a synchrotron source, typically of three orders of magnitude, has a tremendous impact for infrared microspectroscopy of biological and biomedical applications. It has been made clear that infrared signatures are

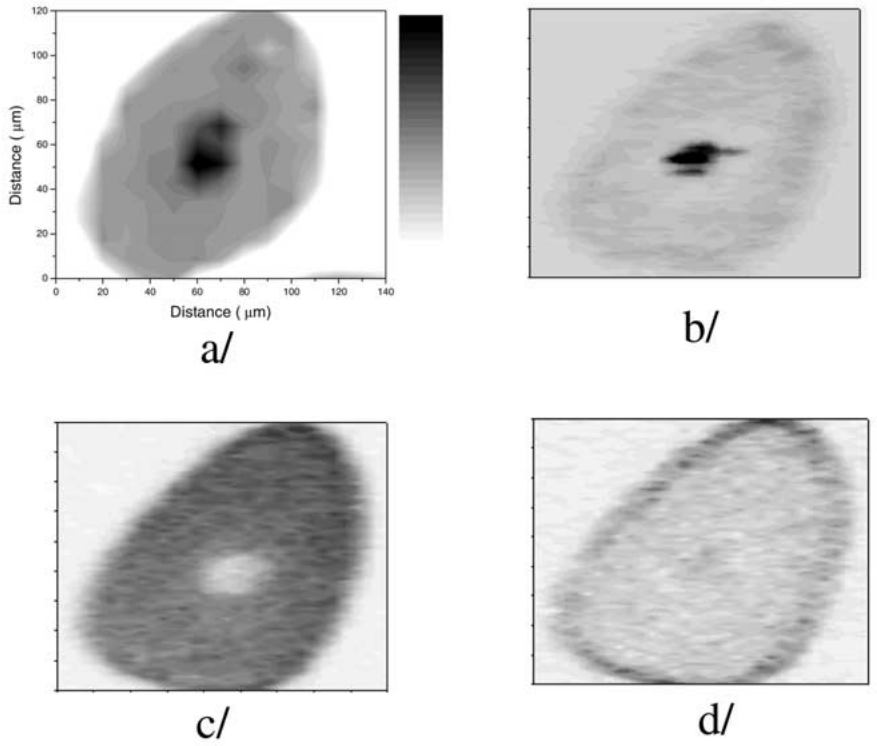

Figure 11. Chemical imaging of a cross-section of hair: **(a)** Infrared chemical image of lipids, **(b)** x-ray image of the Ca profile, **(c)** x-ray image of the S profile, and **(d)** x-ray image of the Cu profile. X-ray images were obtained by X-ray microfluorescence, at photon incident energy of 17 keV (ID22 beamline, ESRF).

potentially suitable for the characterization of samples histology and pathology, without the need for fixatives or stains, when the IR spectra are collected in a spatially resolved fashion, i.e. by using an infrared microscope. The complexity and heterogeneity of the biological samples necessitate a higher spatial resolution. Although micron-scale resolution may not be the ultimate goal, synchrotron-based infrared microspectroscopy has tremendously improved the resolution over a conventional source, allowing analysis of tissue sub-structures (e.g. human hair and skin) and in individual cells. Each of these applications has been examplified in this article. Additionally, the high signal-to-noise spectra obtained allow a much better statistical treatment of the data.

It appears obvious that a combination of probes on the same sample would greatly be beneficial for the understanding of their biochemical composition and classification. Fluorescence-assisted IR microspectroscopy now become an essential tool in the biological and biomedical fields [28]. With the existing synchrotron-based X-ray microscopes at almost every synchrotron facility, combined studies are

now feasible, and efforts need to be undertaken to analyze the same sample area. Experiments such as these are underway at some synchrotron facilities.

Acknowledgements

The authors wish to thank G.P. Williams and G.L. Carr for their valuable input into this collaboration and for their very fruitful discussions. We are particularly thankful to N. Jamin, J.L. Teillaud, Y. Duvault, N. Gross, S. Marull, O. Chubar ,S. Bohic and A.Somogyi for their collaboration and discussions.

References

1. Jackson, M. and Mantsch, H.H.: In: R.A. Myers (ed.), *Encyclopedia of Analytical Chemistry*, John Wiley and Sons Ltd, Chichester, 2000, p. 131–151.
2. Jackson, M. and Mantsch, H.H.: In: M.C. H.H. Mantsch (ed.), *Infrared Spectroscopy of Biomolecules*, Wiley-Liss Inc., Toronto, 1996, p. 311–319.
3. Jackson, M. and Mantsch, H.H.: Molecular Spectroscopy in Biodiagnostics, *Crit. Rev. Biochem. & Mol. Biol.* **30** (1995), 95–102.
4. Naumann, D.: Infrared Spectroscopy in Microbiology, In: R.A. Mayers (ed.), *Encyclopedia of Analytical Chemistry,* John Wiley & Sons Ltd, 2002, p. 102–131.
5. Wetzel, D.L. and LeVine, S.M.: Imaging Molecular Chemistry with Infrared Microscopy, *Science* **285** (1999), 1224–1225.
6. Fabian, H., Jackson, M., Murphy, L., Watson, P.H., Fichtner, I. and Mantsch, H.H.: A Comparative Infrared Spectroscopic Study of Human Breast-Tumors and Breast-Tumor Cell Senografts, *Biospectroscopy* **1** (1995), 37–45.
7. Chiriboga, L., Xie, P., Yee, H., Zarou, D., Zakim, W. and Diem, M.: Infrared Spectroscopy of Human Tissue. IV. Detection of Dysplastic and Neoplastic Changes of Human Cervical Tissue via Infrared Microscopy Cell, *Mol. Biol.* **44** (1998), 219–229.
8. Lasch, P., Boese, M., Pacifico, A. and Diem, M.: FT-IR Spectroscopic Investigations of Single Cells on the Subcellular Level, *Vibrational Spectroscopy* **28** (2002), 147–157.
9. Chalmers, J.M. and Griffiths, P.R.: *Handbook of Vibrational Spectroscopy,* John Wiley and Sons, 2002.
10. Duncan, W.D. and Williams, G.P.: Infrared Synchrotron Radiation from Electron Storage Rings, *Appl. Opt.* **22** (1983), 2914–2923.
11. Winnick, H.: In: *Synchrotron Radiation Research*, Plenum Press, New York, 1980.
12. Chubar, O. and Elleaume, P.: `www.esrf.fr/machine/support/ids/Public/Codes/SRW/srwindex.html`
13. Williams, G.P.: Synchrotron and Free Electron Laser Sources of Infrared Radiation, In: J.M. Chalmers and P.R. Griffiths (eds.), *Handbook of Vibrational Spectroscopy*, John Wiley & Sons, 2001, p. 341–348.
14. Williams, G.P.: Infrared Synchrotron Radiation, Review of Properties and Prospectives, In: G.L. Carr and P. Dumas (eds.), *SPIE – The International Society of Optical Engineering* **3775** (1999), 2–6.
15. Martin, M.C., Tsvetkova, N.M., Crowe, J.H. and McKinney, W.R.: Negligible Sample Heating from Synchrotron Infrared Beam, *Appl. Spectr.* **55** (2001), 111–113.
16. Polack, F., Mercier, R., Nahon, L., Armellin, C., Marx, J.P., Tanguy, M., Couprie, M.E. and Dumas, P.: Optical Design and Performance of the IR Microscope Beamline at SUPERACO-France, In: G.L. Carr and P. Dumas (eds.), *SPIE – The International Society of Optical Engineering* **3775** (1999), 13–21.

17. Carr, G.L., Merlo, O., Munsli, M., Springer, S. and Ho, S.C.: Characterization of the new NSLS Infrared Microspectroscopy Beamline U10B, In: G.L. Carr and P. Dumas (eds.), *SPIE – The International Society of Optical Engineering* **3775** (1999), 22–28.
18. Parker, F.S.: *Applications of Infrared, Raman and Resonance Raman Spectroscopy in Biochemistry*, Plenum Press, New York, 1983.
19. Kreplak, L., Briki, F., Duvault, Y., Doucet, J., Merigoux, C., Leroy, F., Lévêque, J.L., Miller, L., Carr, G.L., Williams, G.P. and Dumas, P.: Profiling Lipids across Caucasian and Afro-American Hair Transverse Cuts, using Synchrotron Infrared Microspectrometry, *Intern. J. Cosm. Sci.* **23**(6) (2001), 369–374.
20. Dumas, P. and Miller, L.: The Use of Synchrotron Infrared Microspectroscopy in Biological and Biomedical Investigations, *Vibrational Spectroscopy* to be published.
21. Bantignies, J.L., Fuchs, G., Carr, G.L., Williams, G.P., Lutz, D. and Marull, S.: Chemical Imaging of Hair by Infrared Microspectroscopy using Synchrotron Radiation, *J. Cosm. Sci.* **51** (2000), 73–90.
22. Mansfield, J.R., McIntosch, L.M., Crowson, A.N., Mantsch, H.H. and Jackson, M.: LDA-Guided Search Engine for the Nonsubjective Analysis of Infrared Microscopic Maps, *Appl. Spectr.* **53** (1999), 1323–1330.
23. McIntosch, L.M., Mansfield, J.R., Crowe, J.H., Mantsch, H.H. and Jackson, M.: *Biospectroscopy* **5** (1999), 265.
24. Elias, P.M., Cooper, E.R., Korc, A. and Brown, B.A.: *J. Invest. Dermatol.* **67** (1981), 291.
25. Gross, N., Marull, S., Fromageot, C., Lebel, M., Baret, J.M., Barbier, A., Ortega, J.M. and Dumas, P.: to be published.
26. Jamin, N., Dumas, P., Moncuit, J., Fridman, W.-H., Teillaud, J.L., Carr, G.L. and Williams, G.P.: Highly Resolved Chemical Imaging of Living Cells by using Synchrotron Infrared Microspectrometry, *Proc. Natl. Acad. Sci. USA* **95** (1998), 4837–4840.
27. Jamin, N., Dumas, P., Moncuit, J., Fridman, W.-H., Teillaud, J.L., Carr, G.L. and Williams, G.P.: Chemical Imaging of Nucleic Acids, Proteins and Lipids of a Single Living Cell. Application of Synchrotron Infrared Microspectrometry in Cell Biology, *Cell. Mol. Biol.* **44** (1998), 9–13.
28. Miller, L., Dumas, P., Jamin, N., Teillaud, J.L., Miklossi, J. and Forro, L.: Combining IR Spectroscopy with Fluorescence Imaging in a Single Microscope: Biomedical Applications using a Synchrotron Infrared Source, *Rev. Sci. Instr.* **73** (2002), 1357–1360.
29. Jamin, N., Miller, L., Moncuit, J., Dumas, P. and Teillaud, J.L.: Chemical Heterogeneity in Cell Death: Combined Synchrotron Infrared and Fluorescence Microscopy Studies of *Single* Apoptotic and Necrotic Cells, submitted (2002).
30. Penner-Hahn, J.E. and Peariso, K.: *Synchr. Radiation News* **13** (2000), 22.
31. Robbins, C.R.: In: Springer-Verlag (ed.), *Chemical and Physical Behavior of Human Hair*, Piscataway, New Jersey, 1988, p. 39–49.
32. Bohic, S., Somogyi, A., Duvault, Y., Susini, J. and Dumas, P.: to be published.